Der Radiologe

Review

Radiologe 2021 · 61 (Suppl 1):S1–S10
https://doi.org/10.1007/s00117-021-00812-8
Accepted: 19 January 2021
Published online: 17 February 2021

E. Wehrse[1,2] · L. Klein[3] · L. T. Rotkopf[1] · W. L. Wagner[4,5] · M. Uhrig[1] · C. P. Heußel[4,5,6] · C. H. Ziener[1] · S. Delorme[1] · S. Heinze[7] · M. Kachelrieß[2,3] · H.-P. Schlemmer[1] · S. Sawall[2,3]

[1] Division of Radiology, German Cancer Research Center, Heidelberg, Germany

[2] Medical Faculty, Ruprecht-Karls-University Heidelberg, Heidelberg, Germany

[3] Division of X-Ray Imaging and Computed Tomography, German Cancer Research Center, Heidelberg, Germany

[4] Department of Diagnostic and Interventional Radiology, University Hospital Heidelberg, Heidelberg, Germany

[5] Translational Lung Research Center Heidelberg, German Center for Lung Research, Heidelberg, Germany

[6] Diagnostic and Interventional Radiology with Nuclear Medicine, Thoraxklinik, University of Heidelberg, Heidelberg, Germany

[7] Institute of Forensic and Traffic Medicine, University Hospital Heidelberg, Heidelberg, Germany

Photon-counting detectors in computed tomography: from quantum physics to clinical practice

Background

Computed tomography (CT) is the most frequently used cross-sectional clinical imaging modality in almost all European countries. In 2017, for example, 15 CT scans were performed per 100 inhabitants in Germany [1]. Since its introduction in the 1970s, CT technology has been continuously improved, as shown by increased scan speed, spatial resolution, and dose efficiency. One of the most promising developments in recent years is a new generation of X-ray detectors. Conventional CT detectors (**Fig. 1a**) consist of distinct detector elements separated by reflecting lamellae [2]. The energy of an incoming X-ray photon is converted into visible light by a scintillator (typically Gd_2O_2S). The optical photons are registered by photodiodes in the detector elements (*detector pixels*), and their number is proportional to the energy of the incoming X-ray photons, i.e., the higher the energy of the X-ray photons, the more optical photons are generated. Hence, the measured signal favors higher energy photons, which diminishes image contrast. Since this detection process is comparatively slow ([3]; **Fig. 1b**), the signals from several incoming photons are summarized, and these detectors are hence referred to as *energy-integrating detectors* (EIDs). Novel *photon-counting detectors* (PCDs) use a semiconductor (typically cadmium telluride [CdTe]) instead of a scintillator ([4]; **Fig. 1c**). Incoming X-ray photons are converted into a measurable charge cloud that is transported to the detector pixels. This detection process is orders of magnitude faster compared to conventional EIDs. In combination with smaller detector pixels, this makes it possible to count single photons at clinical photon flux rates ([2, 5, 6]; **Fig. 1d**). Furthermore, photons can be sorted into several bins according to their energy, allowing for implicit dual- and multi-energy imaging with a single detector [5, 7–9].

Physical advantages

Spatial resolution and image noise. As depicted in **Fig. 1a**, the scintillator in EIDs converts X-ray photons into multiple optical photons. To achieve higher spatial resolution, reflecting lamellas are necessary to guide these photons to the used photodiodes, reducing the active detector area and dose efficiency.

The small detector pixels of PCDs allow for a higher spatial resolution, compared to conventional EIDs. Hence, current PCD CT scanners achieve a higher in-plane and cross-plane resolution [10] if image reconstruction is performed with appropriate voxel sizes and if dedicated ultra-high resolution (UHR) reconstruction kernels are used. Until recently, comparable UHR scans with conventional CT systems could only be performed by using dedicated high resolution hardware combs or grids that significantly reduce dose efficiency [11, 12]. Recently, EIDs with smaller pixels have been introduced into clinical practice, allowing for the acquisition of UHR data without additional grids or combs [13]. Having said that, the reflecting lamellae used in EIDs raise the question of the dose efficiency of these systems. However, publications evaluating this question are not available as yet.

Additionally, the combination of smaller detector elements and a reconstruction to the lower resolution of

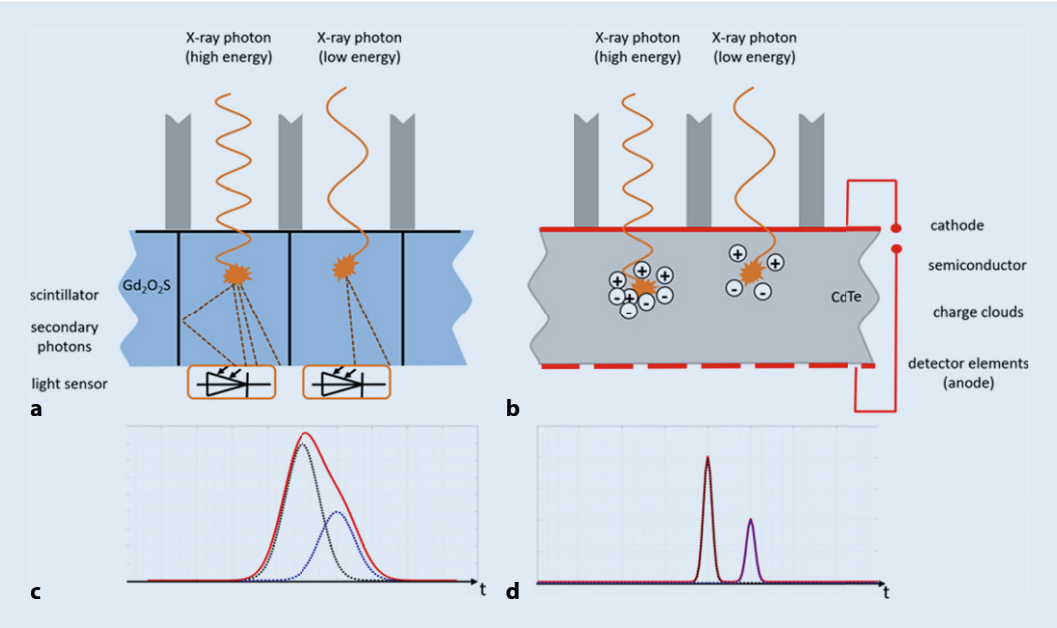

Fig. 1 ◀ Computed tomography detector types: **a** Conventional energy-integrating detector; an incoming X-ray photon is converted to multiple visible photons, which are eventually detected by a light sensor resulting in a wide signal (**c**). **b** Direct conversion of incoming X-ray photons into measurable charge clouds. **d** Photons reaching the detector can be almost simultaneously distinguished by a photon-counting detector. A detailed presentation of the detector element readout modes is provided in ◘ **Fig. 5**. *CdTe* cadmium telluride

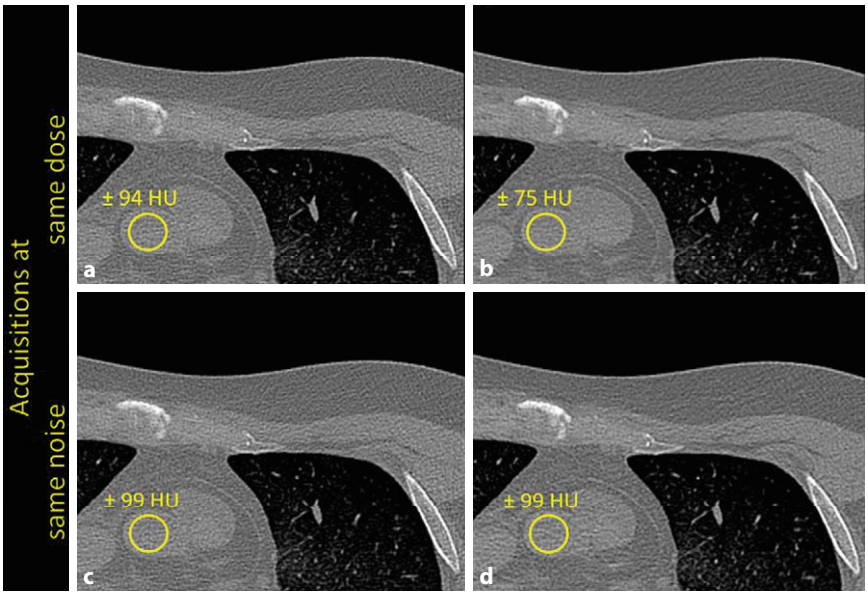

Fig. 2 ▲ Dose- (**a**, **b**) and noise-matched (**c**, **d**) post-mortem thorax examinations using energy-integrating detector (EID) computed tomography (CT) (**a**, **c**) and photon-counting detector (PCD) CT (**b**, **d**) reconstructed to the same spatial resolution (CT window settings: center [C] = 60 HU, width [W] = 360 HU). The CT values (*yellow*) correspond to the standard deviation in the depicted regions of interest. **a**, **b** A direct comparison reveals a 20% noise reduction for PCD over EID (computed tomography dose index volume = 23.0 mGy). **c**, **d** The dose for the PCD CT was 14.6 mGy, while the dose for the EID CT acquisition was 23.0 mGy, i.e., the PCD acquisitions achieve the same noise level with 35% less dose compared to the EID acquisitions

conventional EIDs allows for a reduction in noise and, conversely, radiation dose ([10, 14, 15]; ◘ **Fig. 2**). This effect has been theoretically predicted [16, 17], and recent measurements illustrated radiation dose reductions of up to 65% compared to EIDs at the same noise and spatial resolution [10, 18].

Spectral properties. Since PCDs count single photons, the energy weighting observed in EIDs is overcome. Hence, the effective energy of the detected X-ray spectrum is shifted towards lower energies, increasing soft tissue and iodine contrast. Recent studies illustrate an increase in iodine contrast by up to 37%, which means that the contrast agent dose may be lowered by up to the same amount [19].

State-of-the-art PCD CTs simultaneously acquire at least two energy bins. Reconstructions are typically provided for the entire energy spectrum, i.e., corresponding to a conventional CT image, but individual energy bins can be reconstructed on demand. They might be used to compute images with optimal contrast and contrast-to-noise ratio (CNR), to perform material decomposition similar to dual energy imaging or to reduce beam-hardening and metal artifacts [20, 21].

Furthermore, bin images might be used in combination with potential novel contrast agents to exploit discontinuities in the absorption spectrum (*k-edges*, see ◘ **Fig. 3**), i.e., photons of energies below the k-edge (*low bin*) and above the k-edge (*high bin*) of novel contrast agents containing chemical elements with high atomic numbers (*high-Z elements*) can be separated. This approach promises greatly increased contrast compared to conventional iodinated contrast agents at lower injection volumes and potentially fewer undesired reactions to contrast media. Nonetheless, its effectiveness is also highly dependent on patient size. If more than two energy bins are measured, more than one contrast agent might be used si-

multaneously [22, 23]. However, high-Z contrast agents are not yet available.

Requirements

The SOMATOM CounT (Siemens Healthineers, Erlangen, Germany) [24] is the first available whole-body PCD CT based on a clinical dual-source CT scanner. It houses a PCD as well as a conventional EID, allowing for a comparison of both technologies in the same system (**Fig. 4**). The PCD used in this system provides a native detector pixel size of 225 µm. To limit data transfer demands, the detector usually summarizes the signal of 2 × 2 or 4 × 4 detector pixels (*binning*). The highest spatial resolution is achieved in the UHR mode using a 2 × 2 binning (**Fig. 5a**). Acquisitions in this mode result in a detector pixel size of 0.25 mm at the isocenter. Another mode referred to as *Macro* operates using a 4 × 4 binning, resulting in an overall detector pixel size of 0.50 mm and a spatial resolution that is similar to the EID in the SOMATOM CounT system (**Fig. 5b**). Macro and UHR modes simultaneously acquire two energy bins, while another mode referred to as *Chess* acquires four energy bins (**Fig. 5c**).

Potential clinical applications

The physical characteristics of PCDs have been demonstrated predominantly in well-defined experimental setups. This raises the question of how these findings may impact future patient examinations. The following sections present an overview of the first results obtained by PCD CT prototypes. Where appropriate, the authors provide PCD CT images of an ongoing explorative study at their department (Study number DRKS00017759). Acquisition parameters of this study were adapted from high-resolution EID CT protocols used for temporal bone and inner ear imaging [25, 26]. As such, they are not directly transferable to clinical whole-body or low-dose examinations. A recently published study focusing on sinus and temporal bone examination utilized comparable doses for the EID CT acquisitions and demonstrated dose reductions of more than 60% with PCD [27].

Neuroradiology

The comparison of cranial EID and PCD CT scans of 21 human volunteers revealed that image noise was found to be 13–21% lower in PCD images at the same dose [28], which is in accordance with the results demonstrated in **Fig. 2**. Contrast between gray and white matter was 16% lower in the EID images compared to the PCD images, since EIDs favor high energy photons resulting in a reduction of image contrast.

Nasal sinus and temporal bone

To investigate the imaging performance for very fine anatomical structures, 10 cadaveric temporal bones were scanned using a PCD CT system in UHR mode at clinical dose levels [29]. The recon-

Radiologe 2021 · 61 (Suppl 1):S1–S10 https://doi.org/10.1007/s00117-021-00812-8

E. Wehrse · L. Klein · L. T. Rotkopf · W. L. Wagner · M. Uhrig · C. P. Heußel · C. H. Ziener · S. Delorme · S. Heinze · M. Kachelrieß · H.-P. Schlemmer · S. Sawall

Photon-counting detectors in computed tomography: from quantum physics to clinical practice

Abstract

Over the last decade, a fundamentally new type of computed tomography (CT) detectors has proved its superior capabilities in both physical and preclinical evaluations and is now approaching the stage of clinical practice. These detectors are able to discriminate single photons and quantify their energy and are hence called *photon-counting detectors*. Among the promising benefits of this technology are improved radiation dose efficiency, increased contrast-to-noise ratio, reduced metal artifacts, improved spatial resolution, simultaneous multi-energy acquisitions, and the prospect of multi-phase imaging within a single acquisition using multiple contrast agents. Taking the conventional energy-integrating detectors as a reference, the authors demonstrate the technical principles of this new technology and provide phantom and patient images acquired by a whole-body photon-counting CT. These images serve as a basis for discussing the potential future of clinical CT.

Keywords

CT · Energy-integrating detector · X-ray photons · Ultra-high resolution acquisition · Multi-energy data

Photonenzählende Detektoren in der Computertomographie – von der Quantenphysik zur klinischen Anwendung

Zusammenfassung

Im vergangenen Jahrzehnt hat ein grundlegend neuer Detektortyp in der Computertomographie (CT) seine überlegene Leistungsfähigkeit gezeigt, sowohl in physikalischen als auch in präklinischen Prüfungen. Nun nähert er sich der klinischen Anwendung. Diese Detektoren können einzelne Photonen voneinander unterscheiden und deren Energie messen. Entsprechend werden sie als *Photonenzählende Detektoren* bezeichnet. Zu den vielversprechenden Vorzügen der neuen Technik gehören die verbesserte Strahlendosiseffizienz, ein erhöhtes Kontrast-zu-Rausch-Verhältnis, reduzierte Metallartefakte, eine verbesserte räumliche Auflösung, simultane Multi-Energie-Aufnahmen und die Aussicht auf eine Multiphasenbildgebung mit einer einzigen Aufnahme unter Verwendung mehrerer Kontrastmittel. Mit den konventionellen energieintegrierenden Detektoren als Referenz werden im vorliegenden Beitrag die technischen Grundprinzipien der neuen Technik erläutert. Es werden Phantom- und Patientenbilder präsentiert, die mit photonenzählender Ganzkörper-CT angefertigt wurden. Ausgehend von diesen Bildern werden mögliche Zukunftsaussichten der klinischen CT diskutiert.

Schlüsselwörter

Computertomogramm · Energieintegrierender Detektor · Röntgenstrahlung/Photonen · Ultrahochauflösende Aufnahme · Multi-Energie-Daten

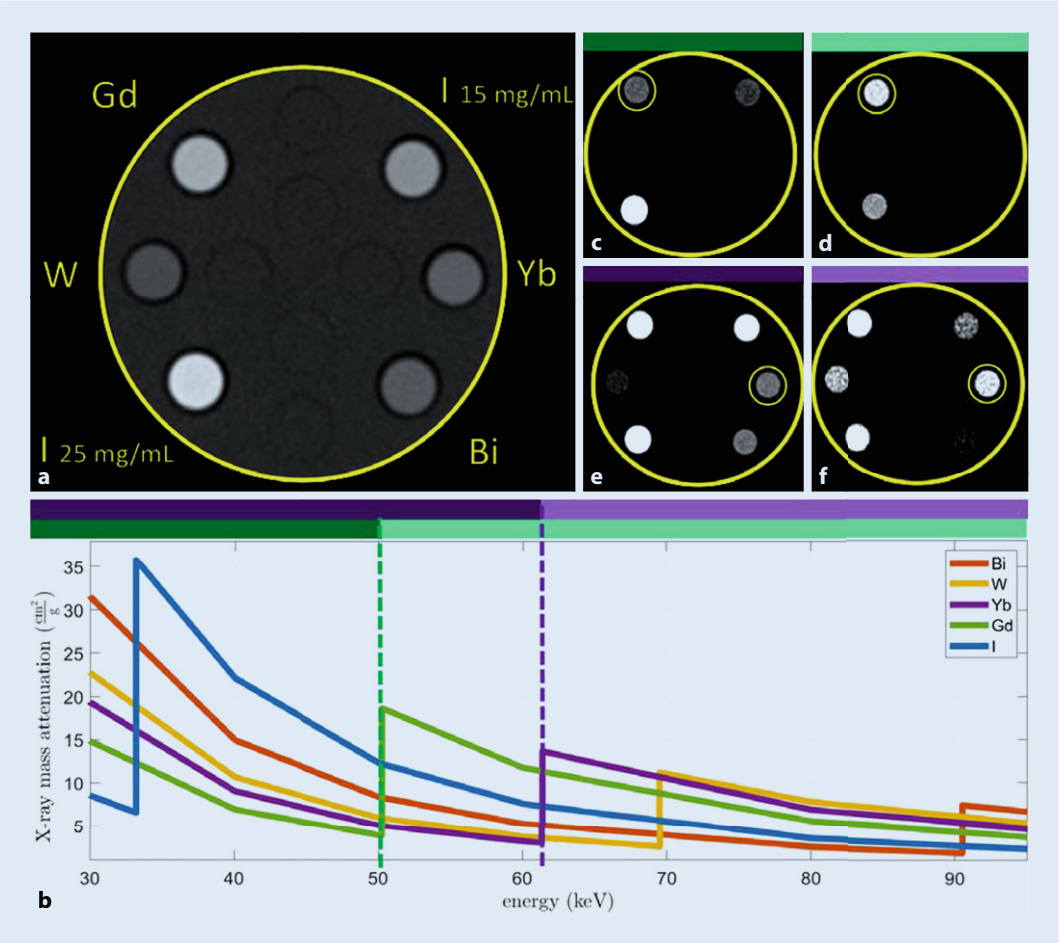

Fig. 3 ◀ **a** Gadolinium (*Gd*), tungsten (wolfram, *W*), iodine (*I*), bismuth (*Bi*), and ytterbium (*Yb*) as potential contrast agents for photon-counting detector computed tomography (low threshold image, bone window). **b** X-ray mass attenuation coefficients of the elements in **a** [50]. Thresholds can be placed near the k-edge of an element to maximize image contrast between low and high bins and hence in the final material decomposition. The k-edge of I is at 33 keV, restricting the applicability of k-edge imaging in clinical practice due to the poor photon statistics in the low energy bin. **c**, **d** Low and high images at 80 kV using a threshold of 50 keV show a contrast improvement of Gd in the high bin. **e**, **f** Low and high bin images using 140 kV and a threshold of 61 keV show an increase in contrast of W and Yb in the higher bin

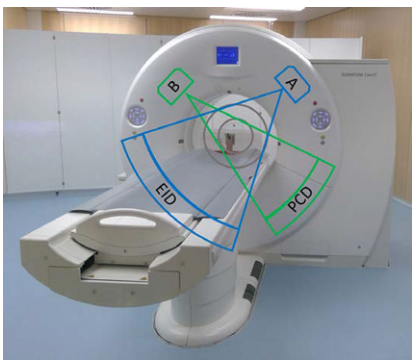

Fig. 4 ▲ The SOMATOM CounT computed tomography (CT) system at the German Cancer Research Center (DKFZ). The position of the energy integrating detector (*EID*) and photon-counting detector (*PCD*) and the corresponding two X-ray sources *A* and *B* are marked in *blue* and *green*. The housing is identical to a conventional clinical CT system

structed images demonstrated superior delineation of temporal microstructures. The three readers, each with at least 10 years of professional experience, preferred these images over the corresponding EID CT images. In combination with a tin filter, PCD UHR acquisitions result in average dose reductions of up to 67% in sinus images obtained in actual patients [27].

Pulmonary and cardiac imaging

Low-dose CT of the thorax is the most important imaging modality in lung cancer screening programs [30]. As a consequence, dose-reduced protocols and additional findings in high-resolution images are of particular interest.

In the case of 20 synthetic pulmonary nodules of up to 12 mm in diameter, the shape and volume quantification as well as the CT number accuracy could be improved by the use of PCD UHR scanning [31]. Superiority to EID CT systems in the assessment of lung nodules and small pulmonary vessels was also demonstrated with a preclinical PCD CT system based on a cadmium zinc telluride (CdZnTe) detector [4]. In this study, in-vivo scans of a rabbit as well as a three-dimensional printed lung phantom with noduli of different sizes and shapes were assessed. For same dose levels, edges and boundaries of sphere-shaped nodules with spikes were more prominent in PCD CT images than in EID CT and high-resolution EID CT images (HR-CT). Improvements in CT-value accuracy and reproducibility of nodules could also be demonstrated in low dose protocols [32]. Furthermore, noise levels in lung parenchyma could be reduced by 11% and CNR in ground-glass nodules and emphysema was improved in PCD CT images, implying prospects to decrease radiation dose for lung cancer screening programs.

These results are consistent with first thorax PCD CT examinations in patients.

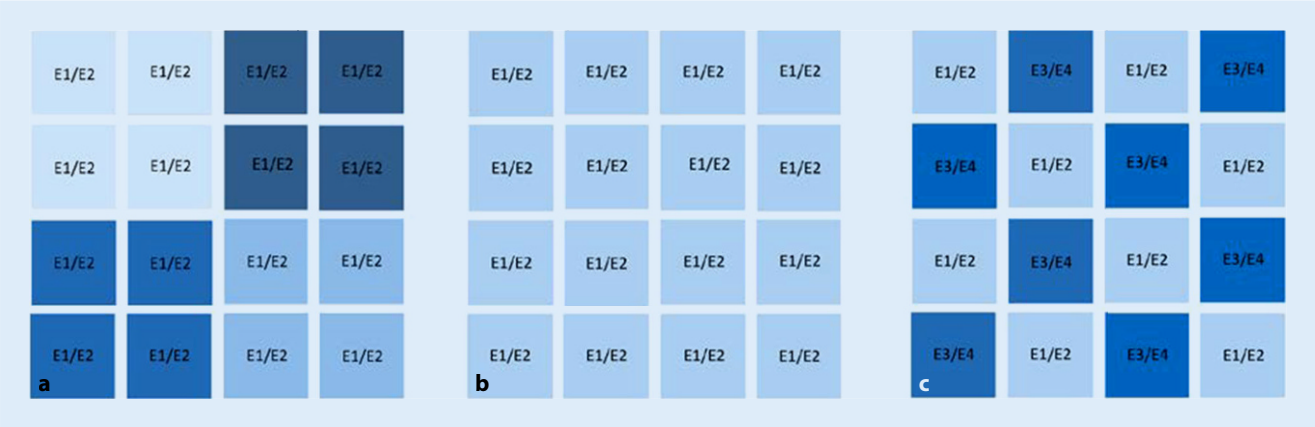

Fig. 5 ▲ Readout modes of the SOMATOM CounT photon-counting detector as a combination of nearby detector elements. Each element is able to discriminate two different energy bins (E_i/ E_j). **a** Ultra-high resolution mode with 2 × 2 binning and **b** macro mode with 4 × 4 binning discriminate two energy bins, while **c** chess mode provides four different energy bins

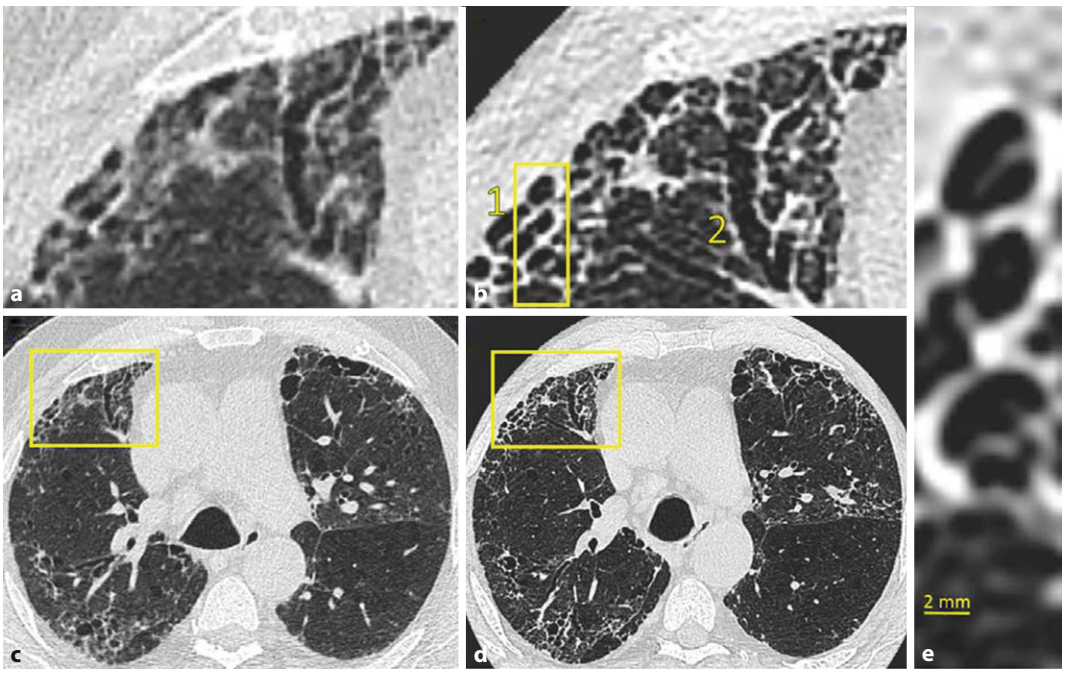

Fig. 6 ▲ Clinical energy-integrating detector (**a**, **c**) and photon-counting detector computed tomography image (**b**, **d**, **e**) in lung window (center [C] = −500 HU, width [W] = 1500 HU) and axial reconstruction demonstrating findings of non-specific interstitial pneumonia in a 71-year-old patient; *1*: honeycombing, *2*: traction bronchiectasis. For an accurate diagnosis, the exclusion of lung parenchyma in these spaces, which requires increased signal-to-noise levels, is of great importance. Acquisition and reconstruction parameters as follows: **a**, **c** SOMATOM Definition AS, 10/2019, pixel size $(0.7\ mm)^3$, computed tomography dose index volume ($CTDI_{vol}$) = 4.34 mGy. **b**, **d**, **e** SOMATOM CounT acquisition in the context of an explorative study 6 days after **a**, **c** $CTDI_{vol}$ = 24.3 mGy, **b**, **d** pixel size 0.5 mm × 0.5 mm × 0.75 mm (transversal [tv] × anterior posterior [ap] × cranio-caudal [cc]), **e** pixel size 0.27 mm × 0.27 mm × 1 mm(tv × ap × cc); all images: I70f reconstruction kernel

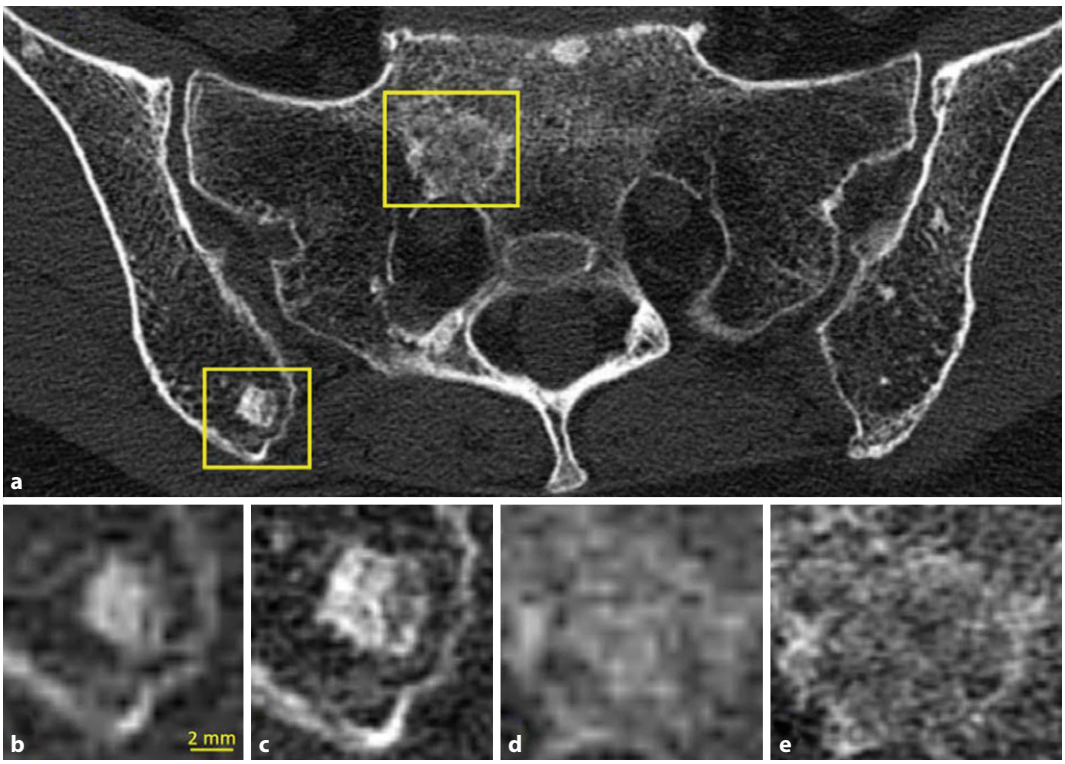

Fig. 7 ▲ Photon-counting detector (PCD) computed tomography (CT) image (**a**, **c**, **e**) and clinical energy-integrating detector image (**b**, **d**) in bone window (center [C] = 500 HU, width [W] = 1500 HU) and axial reconstruction demonstrating osseous metastases in a 68-year-old patient suffering from breast cancer. PCD CT images show improved visualization of the lesions' content with sharper margins. **b**, **c** Osteoplastic lesion in the right iliac bone; **d**, **e** lesion with sclerotic margins ventral of the first sacral foramen. Acquisition and reconstruction parameters as follows: **a**, **c**, **e** SOMATOM CounT acquisition in the context of an explorative study, computed tomography dose index volume ($CTDI_{vol}$) = 24.3 mGy, pixel size 0.27 mm × 0.27 mm × 1 mm (transversal [tv] × anterior posterior [ap] × cranio-caudal [cc]), U70f reconstruction kernel. **b**, **d** SOMATOM Definition Flash, $CTDI_{vol}$ 7.28 mGy, pixel size 0.7 mm × 0.7 mm × 2 mm (tv × ap × cc), B70f reconstruction kernel

In the assessment of thoracic PCD CT images of 30 asymptomatic patients, three experienced radiologists voted in favor of PCD CT images regarding lung nodule image quality and beam hardening artifacts [33]. In a group of 22 patients screened for pulmonary nodules, malignancy, pneumonia, and other pathologies, the detection rate for bronchi of higher order as well as the visualization of small bronchiolar walls could be increased by PCD CT using a 1024 × 1024 matrix [34]. This matrix was also used to visualize microcystic honeycombing in ◘ **Fig. 6e**.

First in-vivo experiments towards cardiac imaging were conducted in a canine model of myocardial infarction by injecting a gadolinium-based contrast agent followed by an iodinated contrast agent 10 min later [35]. Material decomposition of acquired PCD acquisitions allowed for the visualization of first-pass and late myocardial enhancement. Further studies in humans will need to demonstrate the feasibility of a combined first-pass and late-enhancement scan in a single acquisition.

Abdomen and retroperitoneum

Standard abdominal protocols are restricted to one contrast phase per acquisition. This clinically relevant restriction may be overcome by PCD CT and new contrast agents. A comparison of the performance of PCDs and EIDs for abdominal imaging was performed in 15 patients undergoing a contrast-enhanced examination using a SOMATOM CounT [36]. At 2 min after injection of an iodinated contrast agent, an EID scan and an additional 6 s later a dose matched PCD scan was performed using the same patient position. PCD images were comparable to EID images and provided additional multi-energy data. Another study using a canine model demonstrated that these multi-energy data can be used to generate material maps of gadolinium, iodine, and bismuth contrast agents in a single acquisition [23].

Since the location, size, morphology, and composition of kidney stones determine the treatment strategy [37], PCD CT might be able to provide all relevant radiological information to the physician and patient to reach a definitive treatment decision. Ex-vivo examination of 40 kidney stones showed that PCD CT can distinguish stones consisting of uric acid and cysteine, while calcium oxalate monohydrate and apatite could not be reliably distinguished [38]. Even though a direct comparison was not performed with these samples, studies using Dual Energy CT (DECT) resulted in similar conclusions [39, 40]. Additionally, PCD

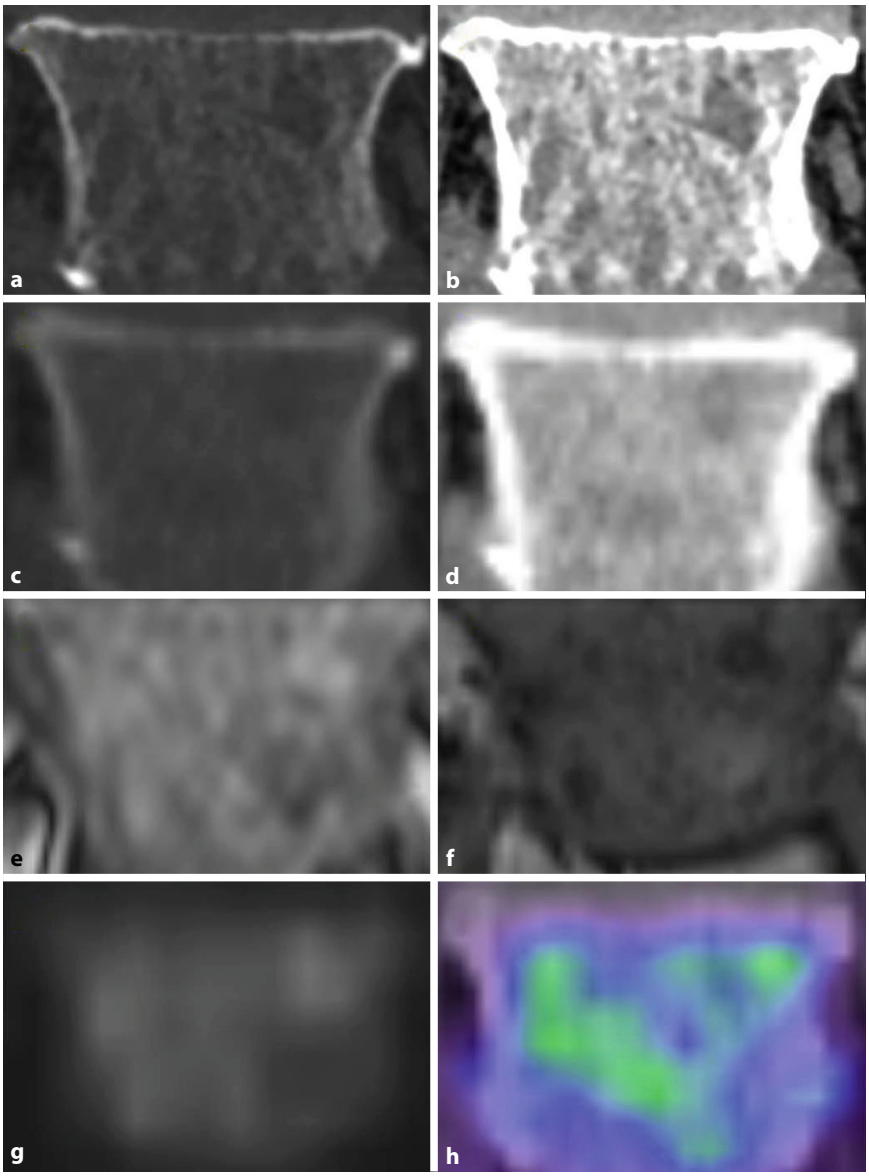

Fig. 8 ▲ Multimodal imaging of the 5th lumbar vertebra in a 64-year-old patient suffering from multiple myeloma. Photon-counting detector (PCD) computed tomogrpahy (CT) images (**a**, **b**) demonstrate diffuse and focal lesions, which are only vaguely visualized in magnetic resonance imaging (MRI) and positron emission tomography (PET) images (**e**-**h**) and cannot be reliably identified in energy-integrating detector CT acquisitions at clinical dose levels and reconstruction parameters (**c**, **d**). In MRI, diffuse T2w-hyperintense (**e**), T1w-hypointense (**f**) infiltrates with increased signal intensity in the diffusion-weighted imaging sequence (**g**) are visualized in accordance with an increased tracer uptake in the F-18 fluorodeoxyglucose (FDG)-PET CT (**h**). CT images in bone (**a**, **c**) and soft tissue window (**b**, **d**), acquisition and reconstruction parameters as follows: **a**, **b** SOMATOM CounT acquisition in the context of an explorative study, pixel size 1 mm × 0.54 mm × 0.54 mm (transversal [tv] × anterior posterior [ap] × cranio-caudal [cc]), I40f, computed tomography dose index volume ($CTDI_{vol}$) = 24.3 mGy. **c**, **d** SOMATOM Emotion, pixel size 1.36 mm × 1.36 mm × 5 mm (cc × tv × ap), B41s, $CTDI_{vol}$ = 4.08 mGy. **a**–**h** In coronal reconstruction. **c**, **d** Courtesy of Dr. Andreas Winterberg from Gemeinschaftspraxis Radiologie und Nuklearmedizin am Beethovenplatz, Saarbrücken. **h** Courtesy of Prof. Dr. Antonia Dimitrakopoulou-Strauss from the Clinical Cooperation Unit Nuclear Medicine at DKFZ, Heidelberg

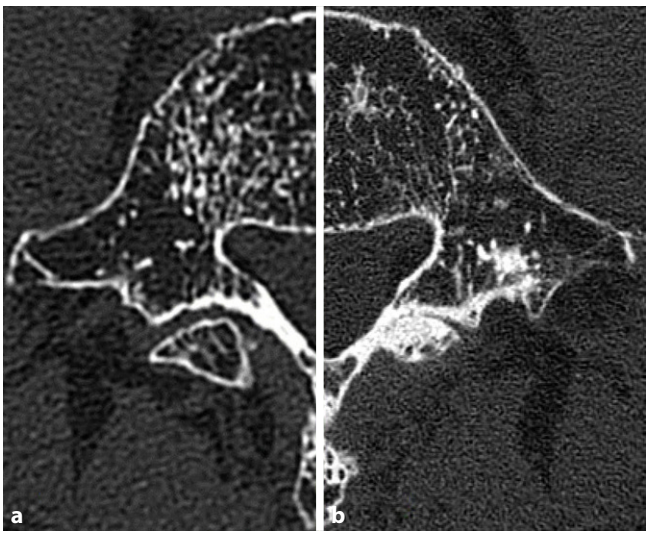

Fig. 9 ▲ Photon-counting detector (PCD) computed tomography (CT) images reconstructed with conventional sharp (**a**) and ultra-high resolution (UHR) U70f kernel (**b**) available for PCD CT, demonstrating the 5th lumbar vertebral body in a 59-year-old patient suffering from multiple myeloma. In the UHR image, the isolated trabeculae and compacta bone do not suffer from over-estimation in terms of CT values and size, enabling an improved assessment of bone marrow and tumorous tissue. Acquisition and reconstruction parameters as follows: SOMATOM CounT, computed tomography dose index volume 24.3 mGy, pixel size 0.27 mm × 0.27 mm × 1 mm (transversal × anterior posterior × cranio-caudal), bone window and axial reconstruction

CT made it possible to automatically detect and characterize stones of less than 3 mm [41].

Crystal arthritis

In a preclinical small animal PCD CT system, a gouty finger and meniscus of the knee from a tissue bank were examined [42], and DECT reconstructions from a conventional clinical CT served as a reference. Both detectors succeeded in detecting monosodium urate crystals. The PCD CT, however, allowed for the delineation of finer structures of aggregated crystals than did conventional CT. In the case of the meniscus, aggregates composed of calcium pyrophosphate could be distinguished from hydroxyapatite crystal deposits, which was validated using polarized light microscopy and X-ray diffraction.

Oncologic imaging of bone marrow

Although research in PCD CT acquisitions of primary bone tumors or metastases is still at a very early stage, first images show qualitative improvements in the visualization of osteoblastic metastases ([43]; ◘ **Fig. 7**). For multiple myeloma, early stages are correlated with a heterogeneous tumor infiltration of bone marrow, which, if located in cancellous bone, can only be detected by magnetic resonance imaging (MRI). For intermediate and advanced stages, however, PCD CT may provide additional information on fine structure, density, and fat content of lesions (◘ **Figs. 8 and 9**).

Radiation therapy

In proton therapy, stopping power ratio (SPR) estimations are crucial for predicting the effectiveness of any treatment and quantifying the potential harm to surrounding tissues. In an experimental setup of nine organic tissue samples, PCD CT showed equal or better results for SPR estimations compared to single energy CT or DECT [44]. Preliminary results in image-guided radiation therapy indicate that PCDs are capable of accurately tracking the motion of lung

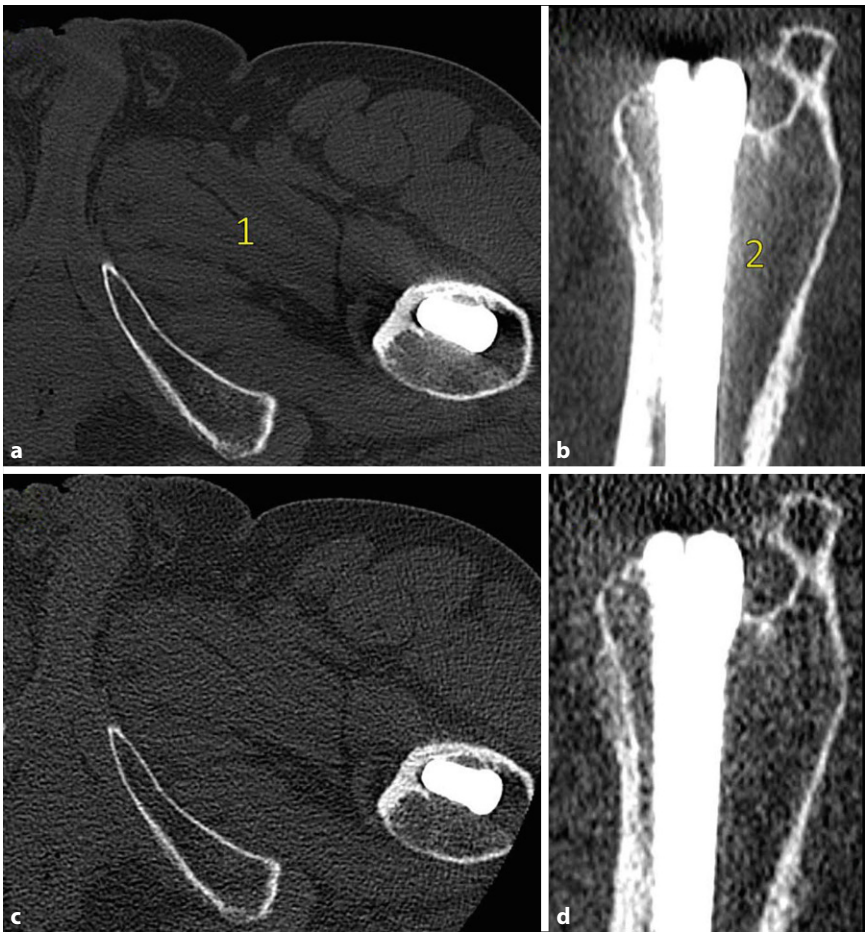

Fig. 10 ▲ Post-mortem energy-integrating detector (EID) computed tomography (CT) (**a**, **b**) and photon-counting detector (PCD) CT (**c**, **d**) acquisitions, reconstructed with a sharp kernel, bone window, computed tomography dose index volume = 34.3 mGy for EID CT and 23.2 mGy for PCD CT. **a** Widespread metal artifacts from a total endoprosthesis (TEP) of the left hip affecting the assessment of the adductor muscles (*1*). **b** Blooming surrounding the TEP makes it difficult to detect signs of loosening in EID images (*2*). **c**, **d** In the high threshold bin of PCD CT data, these two sorts of artifacts are substantially reduced

tumors with only 50 photons per acquisition, if an initial four-dimensional CT scan is provided beforehand [45].

Reduction of metal artifacts

Photons of high energy are more likely to penetrate high density materials compared to low energy photons. Consequently, high energy bin data in PCD CT shows a reduction in beam hardening artifacts and calcium blooming ([46–49]; ◘ **Fig. 10**). In an assessment of 18 different coronary stent types filled with diluted contrast agent, PCD CT images demonstrated a 37% lower increase in lumen attenuation, potentially improving assessment of stent occlusions [49].

Outlook

PCDs for CT have demonstrated superior capabilities when compared to state-of-the-art EIDs. Examples include, but are not limited to, reduced noise, increased spatial resolution, and the acquisition of multi-energy data. These advantages will affect future clinical CT protocols. Contrast-enhanced examinations will benefit from a reduction in administered contrast agent volume and higher image contrast.

Corresponding address

E. Wehrse, MSc MSc
Division of Radiology, German Cancer Research Center
Im Neuenheimer Feld 280,
69120 Heidelberg, Germany
e.wehrse@dkfz-heidelberg.de

Compliance with ethical guidelines

Conflict of interest. E. Wehrse, L. Klein, L. T. Rotkopf, W. L. Wagner, M. Uhrig, C. P. Heußel, C. H. Ziener, S. Delorme, S. Heinze, M. Kachelrieß, H.-P. Schlemmer, and S. Sawall declare that they have no competing interests. ◘ **Fig. 6**, **7**, **8** **and** **9** are from a study for clinical evaluation of a photon-counting CT (German Clinical Trials Register DRKS00017759), approved by the Federal Office for Radiation Protection and all patients gave their informed consent. ◘ **Fig. 2** **and** **10** are post-mortem acquisitions from an ongoing study at DKFZ. Both studies are approved by the Ethics Committee of the Medical Faculty of Heidelberg according to the Declaration of Helsinki of 2013.

This article does not contain any studies with animals performed by any of the authors.

The supplement containing this article is not sponsored by industry.

References

1. (2020) Eurostat healthcare resource statistics—technical resources and medical technology. p. 1–20. https://ec.europa.eu/eurostat/statistics-explained/index.php/Healthcare_resource_statistics_-_technical_resources_and_medical_technology#Use_of_medical_technology. Accessed Internet
2. Kappler S, Glasser F, Janssen S, Kraft E, Reinwand M (2010) A research prototype system for quantum-counting clinical CT. In: ProcSPIE, p 76221Z.
3. Schlegel W, Bille J (2018) Medizinische Physik. Springer, Berlin Heidelberg
4. Kopp FK, Daerr H, Si-Mohamed S, Sauter AP, Ehn S, Fingerle AA et al (2018) Evaluation of a preclinical photon-counting CT prototype for pulmonary imaging. Sci Rep 8(1):1–9
5. Iwanczyk JS, Nygård E, Meirav O, Arenson J, Barber WC, Hartsough NE et al (2009) Photon counting energy dispersive detector arrays for X-ray imaging. IEEE Trans Nucl Sci 56(3):535–542
6. Zambon P, Radicci V, Trueb P, Disch C, Rissi M, Sakhelashvili T et al (2018) Nuclear inst . and methods in physics research , A spectral response characterization of cdTe sensors of different pixel size with the IBEX ASIC. Nucl Instrum Methods Phys Res A 892:106–113
7. Schlomka JP, Roessl E, Dorscheid R, Dill S, Martens G, Istel T et al (2008) Experimental feasibility of multi-energy photon-counting K-edge imaging in pre-clinical computed tomography. Phys Med Biol 53(15):4031–4047
8. Si-Mohamed S, Bar-Ness D, Sigovan M, Cormode DP, Coulon P, Coche E et al (2017) Review of

an initial experience with an experimental spectral photon-counting computed tomography system. Nucl Instrum Methods Phys Res A 873:27–35
9. Cormode DP, Si-Mohamed S, Bar-Ness D, Sigovan M, Naha PC, Balegamire J et al (2017) Multicolor spectral photon-counting computed tomography: In vivo dual contrast imaging with a high count rate scanner. Sci Rep 7(1):1–11
10. Klein L, Dorn S, Amato C, Heinze S, Uhrig M, Schlemmer HP et al (2020) Effects of detector sampling on noise reduction in clinical photon-counting whole-body computed tomography. Invest Radiol 55(2):111–119
11. Kawashima H, Technical Note IK (2019) Performance comparison of ultra-high-resolution scan modes of two clinical computed tomography systems, pp 5–11
12. Flohr TG, Stierstorfer K, Süß C, Schmidt B, Primak AN, McCollough CH (2007) Novel ultrahigh resolution data acquisition and image reconstruction for multi-detector row CT. Med Phys 34(5):1712–1723
13. Onishi H, Hori M, Ota T, Nakamoto A, Osuga K, Tatsumi M et al (2018) Phantom study of in-stent restenosis at high-spatial-resolution CT. Radiology 289(1):255–260
14. Leng S, Rajendran K, Gong H, Zhou W, Halaweish AF, Henning A et al (2018) 150-µm spatial resolution using photon-counting detector computed tomography technology: technical performance and first patient images. Invest Radiol 53(11):655–662
15. Pourmorteza A, Symons R, Henning A, Ulzheimer S, Bluemke DA (2018) Dose efficiency of quarter-millimeter photon-counting computed tomography: first-in-human results. Invest Radiol 53(6):365–372
16. Kachelrieß M, Kalender WA (2005) Presampling , algorithm factors , and noise : considerations for CT in particular and for medical imaging in general. Med Phys 32(5):1321–1334
17. Baek J, Pineda AR, Pelc NJ (2013) To bin or not to bin ? The effect of CT system limiting resolution on noise and detectability To bin or not to bin ? The effect of CT system limiting resolution on noise and detectability. Phys Med Biol 58:1433–1446
18. Leng S, Yu Z, Halaweish A, Kappler S, Hahn K, Henning A, Li Z, Lane J, Levin DL, Jorgensen S, Ritman E, McCollough C (2016) Dose-efficient ultrahigh-resolution scan mode using a photon counting detector computed tomography system. J Med Imaging 3(4):43504
19. Sawall S, Klein L, Amato C, Wehrse E, Dorn S, Maier J et al (2020) Iodine contrast-to-noise ratio improvement at unit dose and contrast media volume reduction in whole-body photon-counting CT. Eur J Radiol 126:108909
20. Nasirudin RA, Mei K, Panchev P, Fehringer A, Pfeiffer F, Rummeny EJ et al (2015) Reduction of metal artifact in single photon-counting computed tomography by spectral-driven iterative reconstruction technique. PLoS ONE 10(5):1–15
21. Willemink MJ, Persson M, Pourmorteza A, Pelc NJ, Fleischmann D (2018) Photon-counting CT: Technical principles and clinical prospects. Radiology 289(2):293–312
22. Kim J, Bar-ness D, Si-mohamed S, Coulon P, Blevis I, Douek P et al (2018) Assessment of candidate elements for development of spectral photon-counting CT specific contrast agents. Sci Rep 8(1):1–12. https://doi.org/10.1038/s41598-018-30570-y
23. Symons R, Krauss B (2017) Photon-counting CT for simultaneous imaging of multiple contrast agents in the abdomen : an in vivo study. Med Phys 44(10):5120–5127
24. Kappler S, Hannemann T, Kraft E, Kreisler B, Niederloehner D (2012) First results from a hybrid prototype CT scanner for exploring benefits of quantum-counting in clinical CT
25. Leng S, Diehn FE, Lane JI, Koeller KK, Witte RJ, Carter RE et al (2015) Temporal bone CT : improved image quality and potential for decreased radiation dose using an ultra-high-resolution scan mode with an iterative reconstruction algorithm. Am J Neuroradiol 36(9):1599–1603
26. McCollough CH, Leng S, Sunnegardh J, Vrieze TJ, Yu L, Lane J et al (2013) Spatial resolution improvement and dose reduction potential for inner ear CT imaging using a z-axis deconvolution technique. Med Phys 40(6):1–9
27. Rajendran K, Voss BA, Zhou W, Tao S, Delone DR, Lane JI et al (2020) Dose reduction for sinus and temporal Bone imaging using photon-counting detector CT with an additional tin filter. Invest Radiol 55(2):91–100
28. Pourmorteza A, Symons R, Reich DS, Bagheri M, Cork TE, Kappler S, Bluemke DA (2017) Photon-counting CT of the brain : in vivo human results and. Am J Neuroradiol 38(12):2257–2263
29. Zhou W, Lane JI, Carlson ML, Bruesewitz MR, Witte RJ, Koeller KK et al (2018) Comparison of a photon-counting-detector CT with an energy-integrating-detector CT for temporal bone imaging: a cadaveric study. Am J Neuroradiol 39(9):1733–1738
30. Tanoue LT, Tanner NT, Gould MKG, Silvestri GA (2015) Lung cancer screening. Am J Respir Crit Care Med 191(1):19–33
31. Zhou W (2017) Lung nodule volume quantification and shape differentiation with an ultra-high resolution technique on a photon-counting detector computed tomography system. J Med Imaging 4(04):1
32. Symons R, Cork TE, Sahbaee P, Fuld MK, Kappler S, Folio LR et al (2017) Low-dose lung cancer screening with photon-counting CT: a feasibility study. Phys Med Biol 62(1):202–213
33. Symons R, Pourmorteza A, Sandfort V, Ahlman MA, Cropper T, Mallek M et al (2017) Feasibility of dose-reduced chest CT with photon-counting detectors: initial results in humans. Radiology 285(3):980–989
34. Bartlett DJ, Koo CW, Bartholmai BJ, Rajendran K, Weaver JM, Halaweish AF et al (2019) High-resolution chest computed tomography imaging of the lungs: impact of 1024 matrix reconstruction and photon-counting detector computed Tomography. Invest Radiol 54(3):129–137
35. Symons R, Cork TE, Lakshmanan MN, Evers R, Davies-Venn C, Rice KA et al (2017) Dual-contrast agent photon-counting computed tomography of the heart: initial experience. Int J Cardiovasc Imaging 33(8):1253–1261
36. Pourmorteza A, Symons R, Sandfort V, Mallek M, Fuld MK, Henderson G et al (2016) Abdominal imaging with contrast-enhanced photon-counting CT: first human experience. Radiology 279(1):239–245
37. Khan SR, Pearle MS, Robertson WG, Gambaro G, Canales BK, Traxer O (2016) Kidney stones. Nat Rev Dis Prim 2(1):1–23
38. Gutjahr R, Polster C, Henning A, Kappler S, Leng S, McCollough CH et al (2017) Dual energy CT kidney stone differentiation in photon counting computed tomography. Proc. SPIE 10132, Medical Imaging 2017: Physics of Medical Imaging, 1013237. https://doi.org/10.1117/12.2252021
39. Ferrero A, Gutjahr R, Halaweish AF, Leng S, Mccollough CH (2018) Characterization of Urinary Stone Composition by Use of Whole-body, Photon-counting Detector CT. Acad Radiol 25(10):1270–1276
40. Fung GSK, Kawamoto S, Matlaga BR, Taguchi K, Zhou X, Fishman EK et al (2012) Differentiation of kidney stones using dual-energy CT with and without a tin filter. Med Phys 198(June):1380–1386
41. Marcus RP, Fletcher JG, Ferrero A, Leng S, Halaweish AF (2018) Detection and characterization of renal stones by using photon-counting—based CT. Radiology 289(2):436–442
42. Stamp LK, Anderson NG, Becce F, Rajeswari M, Polson M, Guyen O et al (2019) Clinical utility of multi-energy spectral photon-counting computed tomography in crystal arthritis. Arthritis Rheumatol 71(7):1158–1162
43. Wehrse E, Klein L, Kachelrieß M, Schlemmer H-P, Ziener C, Wennmann M et al (2020) First experience in man with an ultra-high resolution whole-body photon-counting CT for oncologic imaging. ECR 2020 Book of Abstracts. Insights Imaging 11(Suppl 1):34. https://doi.org/10.1186/s13244-020-00851-0
44. Taasti VT, Hansen DC, Michalak GJ, Deisher AJ, Kruse JJ, Muren LP et al (2018) Theoretical and experimental analysis of photon counting detector CT for proton stopping power prediction. Med Phys 45(11):5186–5196
45. Aschenbrenner KP, Guthier CV, Lyatskaya Y, Boda-Heggemann J, Wenz F, Hesser JW (2017) Positionsschätzung von Lungentumoren mittels Einzelphotonen-Röntgendetektion basierend auf 4D-CT – eine Machbarkeitsstudie. Z Med Phys 27(3):243–254
46. Zhou W, Bartlett DJ, Diehn FE, Glazebrook KN, Kotsenas AL, Carter RE et al (2019) Reduction of metal artifacts and improvement in dose efficiency using photon-counting detector computed tomography and tin filtration. Invest Radiol 54(4):204–211
47. Yu Z, Leng S, Jorgensen SM, Li Z, Gutjahr R, Chen B et al (2016) Evaluation of conventional imaging performance in a research whole-body CT system with a photon-counting detector array. Phys Med Biol 61(4):1572–1595
48. Gutjahr R, Halaweish AF, Yu Z, Leng S, Yu L, Li Z et al (2016) Human imaging with photon counting-based computed tomography at clinical dose levels: Contrast-to-noise ratio and cadaver studies. Invest Radiol 51(7):421–429
49. Mannil M, Hickethier T, Von Spiczak J, Baer M, Henning A, Hertel M et al (2018) Photon-Counting CT: High-Resolution Imaging of Coronary Stents. Invest Radiol 53(3):143–149
50. Seltzer S (1996) Tables of X-ray mass attenuation coefficients and mass energy-absorption coefficients. NISTIR-5632